



28 **Abstract**

29 To better quantify water and energy cycles, numerous efforts to partition evapotranspiration (ET)
30 into evaporation (E) and transpiration (T) have been made over the recent half century. Various methods
31 such as direct measurements, analytical models and satellite-based estimations have been used to separate
32 ET across the field scale to the global scale. One of the analytical methods, isotopic approach, has been
33 often applied in terrestrial ecosystem ET partitioning. The isotopic composition of ET (δ_{ET}) is a crucial
34 parameter in the traditional isotope-based ET partition model, which however has considerable uncertainty.
35 Here we proposed a new method relying on Keeling plot slope (k), and relying on the direct measurements
36 of atmospheric vapor concentration (C_v) and isotopic composition of atmospheric vapor (δ_v), to avoid the
37 direct use of δ_{ET} . Mathematical derivation of the new method was provided, and field observations were
38 used to evaluate the new method. The T/ET results based on the new method agreed well with those using
39 the traditional isotopic method. The new method eliminates the high sensitivity contribution parameter δ_{ET} .
40 In addition, the new method utilized directly measured values and regressive slope of Keeling plot instead
41 of using the interpolated Keeling plot intercept. Our study shows an analytical framework to estimate T/ET
42 based on the Keeling plot slope and direct-measured parameters. The new method potentially reduces the
43 uncertainty of isotope-based ET partition approach.

44

45 **Key words:** ecohydrology, evaporation, evapotranspiration, Keeling plot, stable isotope; transpiration

46

47

48

49

50

51

52

53



54 **1. Introduction**

55 Evapotranspiration (ET) links water, energy, and carbon cycles on land surface (Jung et al., 2010),
56 consisting of evaporation (E) from soil (Sprenger et al., 2016) and open water (Gat et al., 1994), and
57 transpiration (T) from plants (Wang et al., 2012a; Wang et al., 2014). The processes and biological controls
58 of E and T are largely different: T is associated with physiological and biochemical reaction during plant
59 carbon sequestration, while E does not directly attribute to gross primary production and it is not directly
60 affected by biological processes (Scott et al., 2006; Wang et al., 2018; De Deurwaerder et al., 2020). Thus,
61 accurate quantification of T fraction in total ET is of great importance to understand water use efficiency
62 (WUE) from the canopy to the ecosystem scales (Zhou et al., 2014; Zhou et al., 2016). Besides,
63 implementing ET partition improves the comprehending of ecohydrological process, therefore benefits our
64 ability to quantify biological feedbacks on the hydrologic cycle (Newman et al., 2006). Moreover, ET and
65 its components have been used to interpret the vegetation control on ET (Wang et al., 2014) and surface
66 soil moisture control on ET (Cui et al., 2020), as well as to identify some inaccurate estimation of vegetation
67 and soil parameters in global climate model (GCM) (Lawrence et al., 2007; Peñuelas and Filella, 2009).
68 Therefore, ET partition is an important research topic in ecohydrological studies.

69 The attempt to separation E and T began at least in the 1970s (Ritchie, 1972), which initially rely on
70 direct measurements using micro-lysimeter measurements for E (Walker, 1984) and sap flow measurements
71 for T (Swanson and Whitfield, 1981). After Shuttleworth and Wallace (1985) first published ET partition
72 model, numerous analytical models including energy and water balance (ENWATBAL) model (Lascano et
73 al., 1987), soil water energy and transpiration (SWEAT) model (Daamen and Simmonds, 1996), two-source
74 energy balance (TSEB) model (Norman et al., 1995), FAO dual-Kc model (Allen et al., 1998) and isotope
75 model (Yepez et al., 2003) were developed to determine F_T at plot or field scales. Meanwhile, satellite-
76 based estimations made it possible to determine F_T at regional or global scale (Wei et al., 2017; Martens et
77 al., 2017).

78 Hydrogen and oxygen isotopes are natural components of the hydrological cycle. E and T result in



79 different isotopic compositions due to the different isotopic fractionation process (Yepez et al., 2003). Using
80 the isotopic compositions of various ET components, the isotopic approach to estimate F_T has been widely
81 used in woodlands (Sun et al., 2014), grasslands (Cui et al., 2020), croplands (Wen et al., 2016; Lu et al.,
82 2017), and drylands (Sun et al., 2019) ecosystems. Using the isotopic composition of E (δ_E), T (δ_T), and ET
83 (δ_{ET}), F_T can be calculated theoretically based on mass balance (Yakir and Wang, 1996; Yakir and Sternberg,
84 2000). However, previous studies suggested δ_E , δ_T and δ_{ET} estimates are subject to large errors (Xiao et al.,
85 2018), resulting in either over (Sutanto et al., 2012) or under (Wu et al., 2017) F_T estimations compared
86 with direct measurements and other analytical models. According to model sensitivity analysis, the errors
87 of δ_{ET} attributed the most to the potential errors in F_T (Cui et al., 2020). As a result, accurate quantification
88 of δ_{ET} is most crucial to obtain accurate F_T estimate using the isotopic approach.

89 Generally, δ_{ET} is estimated by Keeling plot method (Keeling, 1958; Yakir and Sternberg, 2000), flux-
90 gradient method (Lee et al., 2007) and eddy covariance isotopic flux method (Griffis et al., 2008; Griffis et
91 al., 2010). However, disadvantages remain for all these three methods. Variation in the isotopic composition
92 of atmosphere vapor (δ_v) may be influenced by air masses advection rather than by ET (Lee et al., 2006),
93 which lead to less reliable δ_{ET} estimates using Keeling plot method over a long time period (Good et al.,
94 2012). The representativeness of two heights in flux-gradient method is questionable (Good et al., 2012),
95 as the eddy diffusivity parameter may not be constant at the bottom of the boundary layer where vegetation
96 interacts with turbulent airflow, leading to variable vertical meteorological conditions (Monin and Obukhov,
97 1954). Eddy covariance isotopic flux method may induce many uncertainties when estimating the
98 covariance between isotopic ratios and vertical wind speed, as the information lost in the measured factors
99 (Good et al., 2012). In some case, the δ_{ET} may be underestimated by more than 20% for hydrogen, no matter
100 which method to be adopted (Good et al., 2012; Cui et al., 2020). Inevitably, reducing the uncertainty of
101 δ_{ET} estimate is critically needed.

102 In this paper, we proposed a new method to estimate F_T using a modified isotopic approach without
103 the need of δ_{ET} parameter. This new method relies on the identical instrumental setting for the classical
104 Keeling plot investigations. A detailed derivation of the new method was provided, and the new method



105 was evaluated by comparing the new method with traditional method using field observations. To further
106 assess the new method, a global sensitivity analysis was also conducted for model parameter evaluation.

107

108 2. Materials and Methods

109 2.1 Isotope-based ET partition methods

110 2.1.1 Traditional method

111 Traditionally, by measuring δ_E , δ_T and δ_{ET} , applying a two-source mixing model, F_T based on δ_{ET}
112 ($F_T(\delta_{ET})$ method) can be determined as

$$113 \quad F_T(\delta_{ET}) = \frac{T}{ET} = \frac{\delta_{ET} - \delta_E}{\delta_T - \delta_E} \quad , \quad (1)$$

114 The relationships of δ_E and δ_T were demonstrated by an imaginary graph in **Fig. 1**, which was first proposed
115 by Moreira et al. (1997). Line 1 is idealized Keeling plot line resulting from absolute evaporation, and line
116 2 is that of absolute transpiration. The dashed area between line1 and line 2 typifies all feasible Keeling
117 plot lines mixed with E and T (i.e., ET). The intersection point of line 1 and line 2 indicated the source of
118 ambient vapor. In other words, the y-axis of the intersection point stands for the isotopic composition of
119 ambient vapor (δ_a), and the x-axis of the intersection point stands for the inverse of ambient water vapor
120 concentration ($1/C_a$).

121 The Keeling plot method is often applied to simulate δ_{ET} (Keeling, 1958; Yakir and Sternberg, 2000).
122 Measured values and simulated values can be connected using an isotopic two-source mixture equation:

$$123 \quad \delta_v = \frac{C_a(\delta_a - \delta_{ET})}{C_v} + \delta_{ET} \quad , \quad (2)$$

124 where C_a and C_v are the corresponding concentrations of ambient water vapor and directly measured
125 atmospheric water vapor (i.e., the mixture of ambient water vapor and ET). For a given time, with multiple
126 measurements of C_{vi} and δ_{vi} (the single measurement of the vapor concentration and isotopic composition
127 of water vapor, respectively) collected at various heights during one observation period, the intercept δ_{ET}
128 for this moment from ordinary least squares (OLS) of $1/C_{vi}$ and δ_{vi} is able to be estimated (Zhang et al.,



2011). Therefore, during one observation period, $\delta_v = \frac{1}{m} \sum_{i=1}^m \delta_{v_i}$ and $\frac{1}{C_v} = \frac{1}{m} \sum_{i=1}^m \frac{1}{C_{v_i}}$, where m is the
number of the single measurements (δ_{v_i} , $1/C_{v_i}$) used in Keeling plot relationship. The slope (k) of the linear
Keeling plot is defined as $k=C_a(\delta_a - \delta_{ET})$.

δ_E is often calculated using the Craig–Gordon model (Craig and Gordon, 1965), which considering
both equilibrium fractionation and kinetic fractionation, and considering the diffusion of water vapor from
soil surface to the mixed boundary layer:

$$\delta_E = \frac{\frac{\delta_s}{\alpha} - h\delta_v - \varepsilon^* - (1-h)\varepsilon_k}{(1-h) + (1-h)\frac{\varepsilon_k}{1000}}, \quad (3)$$

where h is relative humidity, δ_s is the isotopic composition of soil liquid water at the evaporating front (0–
5 cm), ε^* and α are both the equilibrium fractionation factor from liquid water to vapor, which connected
by the equation $\varepsilon^*=1000(1-1/\alpha)$. α is estimated by Eq. (4) with soil temperature (T) (Majoube, 1971). The
kinetic fractionation factor (ε_k) is specified by Eq. (5) (Gat, 1996; Wei et al., 2015).

$$\alpha(^{18}O) = \frac{1}{1000} \left(1.137 \times \frac{10^6}{T^2 - 0.4156 \times \frac{10^3}{T - 2.0667}} \right) + 1, \quad (4)$$

$$\varepsilon_k = n \left(1 - \frac{D_i}{D} \right) \times 10^3, \quad (5)$$

where n is isotopic enrichment factor of liquid water during evaporation with a value between 0.5 and 1
(Allison et al., 1985; Gat, 1996). We used a value of 0.67 for the farmland here, similar to what was used
in Wei et al. (2015). D_i/D is the ratio of $^1H_2^{18}O$ molecular diffusion coefficients ratio of water vapor in dry
air, with a value of 0.9691 for ^{18}O (Cappa et al., 2003).

δ_T can also be estimated by chamber method based on Keeling plots (Wang et al., 2010). Following
the basic gas exchange principle (Von Caemmerer and Farquhar, 1981; Song et al., 2015a), the chamber
method was further developed to measured δ_T directly as follows (Wang et al., 2012b):

$$\delta_T = \frac{C_m \delta_m - C_v \delta_v}{C_m - C_v}, \quad (6)$$



150 where C_m and δ_m was the concentration and isotopic composition of the mixed vapor, respectively, which
 151 is consisted of the vapor from ET and from the ambient atmosphere.

152 2.1.2 New ET partition method

153 In this study, we focus on the relationship between k and F_T . A simplified triangle graph was made
 154 (**Fig. 2**) according to **Fig. 1**. $(1/C_x, \delta_x)$ is a random point on the Keeling plot. x , y and z represent the length
 155 of the line segment $(\delta_T - \delta_{ET})$, the line segment $(\delta_{ET} - \delta_E)$ and the line segment $(\delta_{ET} - \delta_x)$, respectively, and
 156 α , β and γ represent the intersectional angle of the line segment $(\delta_T - \delta_{ET})$ and the line segment $(\delta_T - \delta_x)$, the
 157 line segment $(\delta_{ET} - \delta_E)$ and the line segment $(\delta_E - \delta_x)$ and the line segment $(\delta_{ET} - \delta_E)$ and the line segment
 158 $(\delta_{ET} - \delta_x)$, respectively. Based on the law of sines, we have:

$$159 \frac{\sin(\gamma - \alpha)}{x} = \frac{\sin \alpha}{z}, \quad (7)$$

$$160 \frac{\sin(\pi - \gamma - \beta)}{y} = \frac{\sin \beta}{z}. \quad (8)$$

161 When combining Eq (7) and Eq (8), we will come up:

$$162 \frac{x}{y} = \frac{\sin(\gamma - \alpha) \sin \beta}{\sin(\gamma + \beta) \sin \alpha}. \quad (9)$$

163 Equation (9) can be transformed as:

$$164 \frac{x}{y} = \frac{\sin \beta \cos \alpha \sin \gamma - \sin \beta \sin \alpha \cos \gamma}{\sin \alpha \sin \beta \cos \gamma + \sin \alpha \cos \beta \sin \gamma}$$

$$165 = \frac{-\sin \alpha \sin \beta \cot \gamma - \sin \alpha \cos \beta + \sin \alpha \cos \beta + \sin \beta \cos \alpha}{\sin \alpha \sin \beta \cot \gamma + \sin \alpha \cos \beta}$$

$$166 = \frac{\sin(\alpha + \beta)}{\sin \alpha} \frac{1}{\sin \beta \cot \gamma + \cos \beta} - 1, \quad (10)$$

167 As k is the tangent value of the angle of Keeling plot line and x-axis positive direction, it is the minus
 168 tangent value of the angle of Keeling plot line and x-axis negative direction according to supplementary
 169 angles' property. As the angle of Keeling plot line and x-axis negative direction and angle γ are
 170 complementary angles, we have the relationship that $k = -\cot \gamma$. When combining Eq (1) and Eq (10), we
 171 will get:



$$F_T = \frac{\delta_{ET} - \delta_E}{\delta_T - \delta_E} = \frac{y}{x + y} = \frac{1}{1 + \frac{x}{y}} = -\frac{\sin \alpha \sin \beta}{\sin(\alpha + \beta)} k + \frac{\sin \alpha \cos \beta}{\sin(\alpha + \beta)}, \quad (11)$$

where

$$\frac{\sin \alpha \sin \beta}{\sin(\alpha + \beta)} = \frac{1}{\frac{\sin \alpha \cos \beta + \cos \alpha \sin \beta}{\sin \alpha \sin \beta}} = \frac{1}{\cot \alpha + \cot \beta} = \frac{1}{C_x(\delta_T - \delta_E)}, \quad (12)$$

$$\frac{\sin \alpha \cos \beta}{\sin(\alpha + \beta)} = \frac{\sin \alpha \cos \beta}{\sin \alpha \cos \beta + \sin \beta \cos \alpha} = \frac{1}{1 + \frac{\tan \beta}{\tan \alpha}} = \frac{\delta_x - \delta_E}{\delta_T - \delta_E}, \quad (13)$$

As a result, F_T is able to be formed theoretically as

$$F_T(\delta_x) = -\frac{1}{C_x(\delta_T - \delta_E)} k + \frac{\delta_x - \delta_E}{\delta_T - \delta_E}, \quad (14)$$

Because Keeling plot is based on the OLS using all the individual data points ($1/C_{vi}$, δ_{vi}), the regression line passes through the mean values of the $1/C_{vi}$ ($1/C_v$) and δ_{vi} (δ_v) based on the properties of the OLS line (Hogg et al., 2005). That is to say the mean values of ($1/C_v$, δ_v) during any observation period must locate on the Keeling plot line. As such, Eq. (14) can be expressed as the following form ($F_T(\delta_v)$ method) during any observation period:

$$F_T(\delta_v) = -\frac{1}{C_v(\delta_T - \delta_E)} k + \frac{\delta_v - \delta_E}{\delta_T - \delta_E}. \quad (15)$$

2.2 Field Evaluation

2.2.1 Experimental Site

Field Evaluation was conducted in Shiyanghe Experimental Station of China Agricultural University. It is located in Wuwei, Gansu Province, northwestern China ($37^{\circ}85'20''N$, $102^{\circ}85'10''E$; altitude 1581m). The new method was tested in a maize field. The average yearly sunshine duration is more than 3,000 hours, and long-term average yearly temperature is around 8 °C. The region is suffered from water shortage. The groundwater table is more than 30m below the surface. The average yearly evaporation of 2,000 mm (from free water surfaces) against with average yearly precipitation of 164 mm perennially. The soil texture in the experimental site is loamy and sandy loam, with the field capacity of about $0.28 \text{ cm}^3 \text{ cm}^{-3}$.



193 2.2.2 Field Experiment

194 Maize was sowed with row length of 40 cm and column width of 26 cm on 20 April in both 2017
195 and 2018, and harvested on 15 September in both 2017 and 2018. The total area was about 39 hectare, and
196 plant density was around 76,000 plants of maize per hectare. Maize is the primary crop cultivated in the
197 surrounding area. The soil temperature was monitored at 5cm depth. Relative humidity was measured at 2-
198 meter-height with 10-min intervals.

199 The sampling of vapor (atmospheric vapor and mixed vapor) and soil water were conducted from
200 June to August 2017 and 2018 (sampling time points are shown in **Table 1**, which is specified hereinafter).
201 Vapor was collected by four gas traps, and was measured using a water vapor isotope analyzer (L2130-i,
202 Picarro Inc., Sunnyvale, CA, USA) from 7:00 am to 7:00 pm with two hours interval. No.1-No.3 traps were
203 placed at just above the canopy, 2 m and 3 m respectively, which was used to collect the vapor of atmosphere
204 at different heights. While No.4 gas trap was used to collect the mixed vapor. To guarantee a thorough mix
205 of transpired vapor and ambient vapor, a long-term-operated fan was fixed embedded of the chamber,
206 which followed the devise of Song et al. (2015b). The mixed vapor was derived from dynamic plant
207 chamber measurements (**Fig. 3**) at a flow rate of $500\text{--}1500\text{cm}^3\text{ min}^{-1}$. The structure of the chamber was
208 corresponding to the design of Pape et al. (2009). The theoretical basis of this design mainly follows the
209 gas exchange principles invited by Wang et al. (2012b). At each observation time point (last for 15 mins),
210 four times of independent measurements were taken corresponding to No.1–No. 4 sampling inlets. One
211 independent measurement lasted for 225 s. The switch process between two independent measurements
212 were self-acting. Since the analyzer record data every 0.9–1s, about 259–264 values for each inlet was
213 recorded within the circulation. For each 225 s measurement period, No. 195 to No. 253 data points were
214 selected to avoid residual issue and effect of transient pressure variation. As a result, 177 data points were
215 used as $(1/C_{vi}, \delta_{vi})$ from No.1–No.3 traps, and the average values of 59 data points were used as C_m and δ_m
216 respectively from No. 4 gas trap. Vapor specifications ensure the precision of a measurement ranging from
217 1,000 to 50,000 ppm, the precision is 0.040‰–0.25‰ for $\delta^{18}\text{O}$ (Zhao et al., 2019). Our vapor calibration
218 procedure was mainly corresponding to the study by Yuan et al. (2020). The volumes of the chamber was



219 40x60x180 cm³, which was made of acrylic glass. Artificial holes in the minor acrylic glass frame allow
220 the device of inlet and outlet porthole. The soil samples were drilled by a soil auger at the depths of 0–5
221 cm. Pure soil liquid water was extracted by a cryogenic vacuum extraction system (LI-2000, LICA United
222 Technology, China), and the extraction method is guided by Orłowski et al. (2013). The δ_s values were
223 measured by the same isotope analyzer (L2130-i, Picarro Inc., Sunnyvale, CA, USA) in liquid water model.
224 δ_s calibration process mainly obeyed the study by Wu et al. (2017). The isotopic compositions values
225 relative to the Standard Mean Ocean Water (SMOW).

226 As our water vapor isotope analyzer was occupied due to maintenance and other experiments, twelve
227 days were chosen to conduct ET partition observation. In each day, the observation started at 7:00 am and
228 end up with 7:00 pm, conducting in 2 hours interval. Overall, we have 84 experimental data sets (**Table 1**).
229 A quantity control filter was used on $F_T(\delta_{ET})$ and $F_T(\delta_v)$, which excluded the values beyond the range (0,1).

230 2.2.3 Global Sensitivity Analysis

231 A global sensitivity analysis was conducted for both two methods to determine the influence of a set
232 of parameters had on predicting $F_T(\delta_{ET})$ and $F_T(\delta_v)$. A Sobol-method-based (Zhang et al., 2015) software,
233 Crystal Ball (Oracle Inc., Redwood City, CA), was used to quantify the contribution of each input parameter
234 to the change of modeling results. The parameter interactions were considered in this approach. Running
235 the software, a Monte Carlo simulation (Bhat and Kumar, 2008) was implemented to supply random
236 variation data trials within the observed range. In the simulation, 10,000 trials were operated for each
237 parameter in both $F_T(\delta_{ET})$ method and $F_T(\delta_v)$ method, as well as 10,000 times subsampling input for each
238 parameter, represented by their mean values and standard deviations among all of the observation time
239 points under an assumed normal distribution (Cui et al., 2020). After analyzing the pattern of these 10,000
240 trials of data derived from Monte Carlo simulation, a distribution of predicted $F_T(\delta_{ET})$ and $F_T(\delta_v)$ was able
241 to be shown. In this study, the mean standard deviation of predicted $F_T(\delta_{ET})$ and $F_T(\delta_v)$ was 0.02 both. Finally,
242 the software produced the contribution of each input parameter to the variability of results. The greater of
243 the percentage value, the more sensitive a model output variable is to that particular parameter.



244 3. Results and Discussion

245 3.1 Comparisons of the new method with the traditional method

246 Among all observation time points, the average δ_{ET} , δ_T , δ_E , δ_v and C_v values are $-11.79 \pm 2.34\%$, -8.50
247 $\pm 1.98\%$, $-28.75 \pm 6.96\%$, $-13.47 \pm 2.00\%$ and 19284.02 ± 5281.09 ppm, respectively (**Table 1**). After the
248 quality control (see section 2.2.2) to exclude the F_T values outside the range (0, 1), 94.0% and 96.4% of
249 $F_T(\delta_{ET})$ and $F_T(\delta_v)$ values remain. Finally, 79 data points overlapped between $F_T(\delta_{ET})$ and $F_T(\delta_v)$ methods.
250 The average $F_T(\delta_{ET})$ and $F_T(\delta_v)$ across all time points were 0.81 ± 0.10 and 0.82 ± 0.12 . The F_T results from
251 the new method agreed well with the results using the traditional method (**Fig. 4**), which supports the
252 validity of the mathematical derivation of the new method using field observations.

253 3.2 The advantages of the new method compared with the traditional method

254 3.2.1 The elimination of high sensitivity contribution parameter δ_{ET}

255 Global sensitivity analysis was conducted for both $F_T(\delta_{ET})$ method (**Fig. 5a**) and $F_T(\delta_v)$ method (**Fig.**
256 **5b**). As for the traditional method, δ_{ET} contributed to 59% of the sensitivity of F_T , significantly larger than
257 those of δ_T and δ_E . The high sensitivity contribution of parameter δ_{ET} was also reported by a previous study
258 (Cui et al., 2020). Generally, great uncertainty of δ_{ET} was revealed in Keeling plot method, flux-gradient
259 method and eddy covariance isotopic flux method (Good et al., 2012), which resulted in large F_T uncertainty
260 when δ_{ET} was used in the traditional method on the basis of sensitivity analysis in our study and others'
261 research (Cui et al., 2020). While in the new method, the parameter with the largest sensitivity contribution
262 was k (46%). This result indicated that Keeling-plot-related parameters (δ_{ET} and k) brought most of the
263 uncertainty to estimate F_T . At the same time, using k rather than δ_{ET} would diminish the uncertainty result
264 from Keeling plot since k can be directly calculated using observations without the need of extrapolation
265 to obtain the intercept δ_{ET} . The second largest sensitivity contribution in the new method was δ_v (27%), a
266 direct measured parameter instead of a simulated value in the traditional method. Meanwhile, the sensitivity
267 contributions of parameter δ_E and δ_T were reduced using the new method (7% and 18%) compared with the
268 traditional method (12% and 29%). It was thus favorable for $F_T(\delta_v)$ method for using a direct measured



269 parameter δ_v , and it will reduce the uncertainty of F_T .

270 3.2.2 The new method avoids extrapolation of Keeling plot

271 One of the limitations of the Keeling plot is that it requires extrapolation far beyond the measured
272 range of data points to the y-axis to obtain the intercept δ_{ET} (Pataki et al., 2003). Geometrically, data points
273 ($1/C_{vi}$, δ_{vi}) are always assembled in a restricted area, which is distant to the potential intercept point of the
274 Keeling plot. In some cases, the extrapolation distance will be 8-10 times of original $1/C_{vi}$ range (Quade et
275 al., 2018), such that small uncertainties in the OLS regression slope result in large uncertainties in the
276 intercept δ_{ET} (Tans, 1998). Our result of high sensitivity of δ_{ET} also supports this point. To make matters
277 worse, to meet the assumption of Keeling plot of constant slope and intercept (Wang et al., 2013), one of
278 the principles is to shorten the observation period to obtain data points ($1/C_{vi}$, δ_{vi}) in a relatively short
279 interval, such as 30 minutes (Good et al., 2012; Xiao et al., 2018). However, short interval data points ($1/C_{vi}$,
280 δ_{vi}) may also shorten the $1/C_{vi}$ range, which further increases the extrapolation distance to the y-axis. In
281 such cases, it is more dependable to use parameters derived from nearby data point ($1/C_{vi}$, δ_{vi}) than an
282 interpolated intercept.

283 4. Conclusions

284 In this study, we established a new isotopic based method to quantify F_T ($F_T(\delta_v)$). The $F_T(\delta_v)$ method
285 was derived based on the law of sines. The new method estimated F_T using the modeled parameter k derived
286 from Keeling plot relationship, and direct measured parameters C_v and δ_v . Evaluated by observation data,
287 the linear regression showed the new $F_T(\delta_v)$ method results agreed well with the results from the traditional
288 $F_T(\delta_{ET})$ method. The new method avoids the use of high sensitivity contribution parameter δ_{ET} . A direct
289 measured parameter δ_v in $F_T(\delta_v)$ method would reduce the uncertainty of F_T simulation. Using the
290 parameters derived from direct measurements rather than extrapolation in Keeling plots, the new method
291 should be more dependable. This study provides an analytical framework to estimate F_T using a novel
292 method based on existing Keeling plot instrumentations. The new method potentially reduces the
293 uncertainty of isotope-based ET partition approach.



294 5. Acknowledgements

295 We acknowledge support from the National Natural Science Foundation of China (51725904,
296 51621061, 51861125103), the National Key Research Program (2016YFC0400207), the Discipline
297 Innovative Engineering Plan (111 Program, B14002), the Research Innovation Fund for Graduate Students
298 of CAU (2020XYZC39A), and the President's International Research Awards from Indiana University and
299 the Division of Earth Sciences of National Science Foundation (EAR-1554894).

300 6. Code and Data Availability

301 Code and data are available on request.

302 7. Author Contribution

303 YY, LW and TD conceptualized the main research questions. YY and WL collected the data. YY
304 performed the data analyses. YY and LW wrote the first draft. WJ contributed to additional analyses on the
305 new method. All the authors contributed ideas and edited the manuscript.

306 8. Competing Interests

307 There authors declare no competing interests.

308 9. References

- 309 Allen, R. G., Pereira, L. S., Raes, D., and Smith, M.: Crop evapotranspiration-Guidelines for computing
310 crop water requirements-FAO Irrigation and drainage paper 56, **Fao, Rome**, 300, D05109, 1998.
- 311 Allison, G., Gat, J. R., and Leaney, F. W.: The relationship between deuterium and oxygen-18 delta values
312 in leaf water, **Chemical Geology: Isotope Geoscience Section**, 58, 145-156, 1985.
- 313 Bhat, A., and Kumar, A.: Application of the Crystal Ball® software for uncertainty and sensitivity analyses
314 for predicted concentration and risk levels, **Environmental Progress**, 27, 289-294, 2008.
- 315 Cappa, C. D., Hendricks, M. B., DePaolo, D. J., and Cohen, R. C.: Isotopic fractionation of water during
316 evaporation, **Journal of Geophysical Research: Atmospheres**, 108, 4525, 2003.
- 317 Craig, H., and Gordon, L. I.: Deuterium and oxygen 18 variations in the ocean and the marine atmosphere,
318 9, 1965.
- 319 Cui, J., Tian, L., Wei, Z., Huntingford, C., Wang, P., Cai, Z., Ma, N., and Wang, L.: Quantifying the controls
320 on evapotranspiration partitioning in the highest alpine meadow ecosystem, **Water Resources**
321 **Research**, 56, e2019WR024815, 2020.
- 322 Daamen, C. C., and Simmonds, L. P.: Measurement of evaporation from bare soil and its estimation using
323 surface resistance, **Water Resources Research**, 32, 1393-1402, 1996.
- 324 De Deurwaerder, H., Visser, M. D., Detto, M., Boeckx, P., Meunier, F., Zhao, L., Wang, L., and Verbeeck,
325 H.: Diurnal variation in the isotope composition of plant xylem water biases the depth of root-water
326 uptake estimates, **Biogeosciences Discussions**, 1-48, 2020.



- 327 Gat, J. R., Bowser, C. J., and Kendall, C.: The contribution of evaporation from the Great Lakes to the
328 continental atmosphere: estimate based on stable isotope data, **Geophysical Research Letters**, 21,
329 557-560, 1994.
- 330 Gat, J. R.: Oxygen and hydrogen isotopes in the hydrologic cycle, **Annual Review of Earth and Planetary**
331 **Sciences**, 24, 225-262, 1996.
- 332 Good, S. P., Soderberg, K., Wang, L., and Caylor, K. K.: Uncertainties in the assessment of the isotopic
333 composition of surface fluxes: A direct comparison of techniques using laser-based water vapor
334 isotope analyzers, **Journal of Geophysical Research: Atmospheres**, 117, D15301, 2012.
- 335 Griffis, T. J., Sargent, S., Baker, J., Lee, X., Tanner, B., Greene, J., Swiatek, E., and Billmark, K.: Direct
336 measurement of biosphere-atmosphere isotopic CO₂ exchange using the eddy covariance technique,
337 **Journal of Geophysical Research: Atmospheres**, 113, D08304, 2008.
- 338 Griffis, T. J., Sargent, S., Lee, X., Baker, J., Greene, J., Erickson, M., Zhang, X., Billmark, K., Schultz, N.,
339 and Xiao, W.: Determining the oxygen isotope composition of evapotranspiration using eddy
340 covariance, **Boundary-layer Meteorology**, 137, 307-326, 2010.
- 341 Hogg, R. V., McKean, J., and Craig, A. T.: Introduction to mathematical statistics, Pearson Education, 2005.
- 342 Jung, M., Reichstein, M., Ciais, P., Seneviratne, S. I., Sheffield, J., Goulden, M. L., Bonan, G., Cescatti, A.,
343 Chen, J., and De Jeu, R.: Recent decline in the global land evapotranspiration trend due to limited
344 moisture supply, **Nature**, 467, 951-954, 2010.
- 345 Keeling, C. D.: The concentration and isotopic abundances of atmospheric carbon dioxide in rural areas,
346 **Geochimica et Cosmochimica Acta**, 13, 322-334, 1958.
- 347 Lascano, R., Van Bavel, C., Hatfield, J., and Upchurch, D.: Energy and Water Balance of a Sparse Crop:
348 Simulated and Measured Soil and Crop Evaporation 1, **Soil Science Society of America Journal**,
349 51, 1113-1121, 1987.
- 350 Lawrence, D. M., Thornton, P. E., Oleson, K. W., and Bonan, G. B.: The partitioning of evapotranspiration
351 into transpiration, soil evaporation, and canopy evaporation in a GCM: Impacts on land-atmosphere
352 interaction, **Journal of Hydrometeorology**, 8, 862-880, 2007.
- 353 Lee, X., Smith, R., and Williams, J.: Water vapour ¹⁸O/¹⁶O isotope ratio in surface air in New England,
354 USA, **Tellus B: Chemical and Physical Meteorology**, 58, 293-304, 2006.
- 355 Lee, X., Kim, K., and Smith, R.: Temporal variations of the ¹⁸O/¹⁶O signal of the whole-canopy
356 transpiration in a temperate forest, **Global Biogeochemical Cycles**, 21, GB3013, 2007.
- 357 Lu, X., Liang, L. L., Wang, L., Jenerette, G. D., McCabe, M. F., and Grantz, D. A.: Partitioning of
358 evapotranspiration using a stable isotope technique in an arid and high temperature agricultural
359 production system, **Agricultural Water Management**, 179, 103-109, 2017.
- 360 Majoube, M.: Fractionnement en oxygene 18 et en deuterium entre l'eau et sa vapeur, **Journal de Chimie**
361 **Physique**, 68, 1423-1436, 1971.
- 362 Martens, B., Gonzalez Miralles, D., Lievens, H., Van Der Schalie, R., De Jeu, R. A., Fernández-Prieto, D.,
363 Beck, H. E., Dorigo, W., and Verhoest, N.: GLEAM v3: Satellite-based land evaporation and root-
364 zone soil moisture, **Geoscientific Model Development**, 10, 1903-1925, 2017.
- 365 Monin, A. S., and Obukhov, A. M.: Basic laws of turbulent mixing in the surface layer of the atmosphere,
366 **Contrib. Geophys. Inst. Acad. Sci. USSR**, 151, e187, 1954.
- 367 Moreira, M., Sternberg, L., Martinelli, L., Victoria, R., Barbosa, E., Bonates, L., and Nepstad, D.:
368 Contribution of transpiration to forest ambient vapour based on isotopic measurements, **Global**
369 **Change Biology**, 3, 439-450, 1997.
- 370 Newman, B. D., Wilcox, B. P., Archer, S. R., Breshears, D. D., Dahm, C. N., Duffy, C. J., McDowell, N.
371 G., Phillips, F. M., Scanlon, B. R., and Vivoni, E. R.: Ecohydrology of water-limited environments:
372 A scientific vision, **Water Resources Research**, 42, W06302, 2006.
- 373 Norman, J. M., Kustas, W. P., and Humes, K. S.: Source approach for estimating soil and vegetation energy
374 fluxes in observations of directional radiometric surface temperature, **Agricultural and Forest**
375 **Meteorology**, 77, 263-293, 1995.
- 376 Orłowski, N., Frede, H.-G., Brüggemann, N., and Breuer, L.: Validation and application of a cryogenic



- 377 vacuum extraction system for soil and plant water extraction for isotope analysis, **Journal of Sensors**
378 **and Sensor Systems**, 2, 179-193, 2013.
- 379 Pape, L., Ammann, C., Nyfeler-Brunner, A., Spirig, C., Hens, K., and Meixner, F.: An automated dynamic
380 chamber system for surface exchange measurement of non-reactive and reactive trace gases of
381 grassland ecosystems, **Biogeosciences**, 6, 405-429, 2009.
- 382 Pataki, D., Ehleringer, J., Flanagan, L., Yakir, D., Bowling, D., Still, C., Buchmann, N., Kaplan, J., and
383 Berry, J.: The application and interpretation of Keeling plots in terrestrial carbon cycle research,
384 **Global Biogeochemical Cycles**, 17, 1022, 2003.
- 385 Peñuelas, J., and Filella, I.: Phenology feedbacks on climate change, **Science**, 324, 887-888, 2009.
- 386 Quade, M., Brüggemann, N., Graf, A., Vanderborcht, J., Vereecken, H., and Rothfuss, Y.: Investigation of
387 kinetic isotopic fractionation of water during bare soil evaporation, **Water Resources Research**, 54,
388 6909-6928, 2018.
- 389 Ritchie, J. T.: Model for predicting evaporation from a row crop with incomplete cover, **Water Resources**
390 **Research**, 8, 1204-1213, 1972.
- 391 Scott, R. L., Huxman, T. E., Cable, W. L., and Emmerich, W. E.: Partitioning of evapotranspiration and its
392 relation to carbon dioxide exchange in a Chihuahuan Desert shrubland, **Hydrological Processes**, 20,
393 3227-3243, 2006.
- 394 Shuttleworth, W. J., and Wallace, J.: Evaporation from sparse crops - an energy combination theory,
395 **Quarterly Journal of the Royal Meteorological Society**, 111, 839-855, 1985.
- 396 Song, X., Loucos, K. E., Simonin, K. A., Farquhar, G. D., and Barbour, M. M.: Measurements of
397 transpiration isotopologues and leaf water to assess enrichment models in cotton, **New Phytologist**,
398 206, 637-646, 2015a.
- 399 Song, X., Simonin, K. A., Loucos, K. E., and Barbour, M. M.: Modelling non-steady-state isotope
400 enrichment of leaf water in a gas-exchange cuvette environment, **Plant, Cell & Environment**, 38,
401 2618-2628, 2015b.
- 402 Sprenger, M., Leistert, H., Gimbel, K., and Weiler, M.: Illuminating hydrological processes at the soil-
403 vegetation-atmosphere interface with water stable isotopes, **Reviews of Geophysics**, 54, 674-704,
404 2016.
- 405 Sun, S., Meng, P., Zhang, J., Wan, X., Zheng, N., and He, C.: Partitioning oak woodland evapotranspiration
406 in the rocky mountainous area of North China was disturbed by foreign vapor, as estimated based on
407 non-steady-state ^{18}O isotopic composition, **Agricultural and Forest Meteorology**, 184, 36-47, 2014.
- 408 Sun, X., Wilcox, B. P., and Zou, C. B.: Evapotranspiration partitioning in dryland ecosystems: A global
409 meta-analysis of in situ studies, **Journal of Hydrology**, 576, 123-136, 2019.
- 410 Sutanto, S., Wenninger, J., Coenders-Gerrits, A., and Uhlenbrook, S.: Partitioning of evaporation into
411 transpiration, soil evaporation and interception: a comparison between isotope measurements and a
412 HYDRUS-1D model, **Hydrology and Earth System Sciences**, 16, 2605-2616, 2012.
- 413 Swanson, R., and Whitfield, D.: A numerical analysis of heat pulse velocity theory and practice, **Journal**
414 **of Experimental Botany**, 32, 221-239, 1981.
- 415 Tans, P. P.: Oxygen isotopic equilibrium between carbon dioxide and water in soils, **Tellus B**, 50, 163-178,
416 1998.
- 417 Von Caemmerer, S. V., and Farquhar, G. D.: Some relationships between the biochemistry of photosynthesis
418 and the gas exchange of leaves, **Planta**, 153, 376-387, 1981.
- 419 Walker, G.: Evaporation from wet soil surfaces beneath plant canopies, **Agricultural and Forest**
420 **Meteorology**, 33, 259-264, 1984.
- 421 Wang, L., Caylor, K. K., Villegas, J. C., Barron-Gafford, G. A., Breshears, D. D., and Huxman, T. E.:
422 Partitioning evapotranspiration across gradients of woody plant cover: Assessment of a stable isotope
423 technique, **Geophysical Research Letters**, 37, L09401, 2010.
- 424 Wang, L., d'Odorico, P., Evans, J., Eldridge, D., McCabe, M., Caylor, K., and King, E.: Dryland
425 ecohydrology and climate change: critical issues and technical advances, **Hydrology and Earth**
426 **System Sciences**, 16, 2585-2603, 2012a.



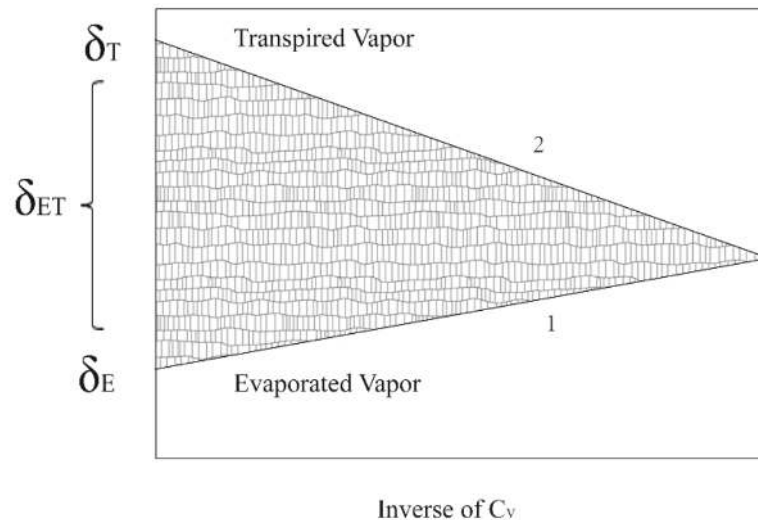
- 427 Wang, L., Good, S. P., Caylor, K. K., and Cernusak, L. A.: Direct quantification of leaf transpiration isotopic
428 composition, **Agricultural and Forest Meteorology**, 154, 127-135, 2012b.
- 429 Wang, L., Niu, S., Good, S. P., Soderberg, K., McCabe, M. F., Sherry, R. A., Luo, Y., Zhou, X., Xia, J., and
430 Caylor, K. K.: The effect of warming on grassland evapotranspiration partitioning using laser-based
431 isotope monitoring techniques, **Geochimica et Cosmochimica Acta**, 111, 28-38, 2013.
- 432 Wang, L., Good, S. P., and Caylor, K. K.: Global synthesis of vegetation control on evapotranspiration
433 partitioning, **Geophysical Research Letters**, 41, 6753-6757, 2014.
- 434 Wang, P., Li, X. Y., Wang, L., Wu, X., Hu, X., Fan, Y., and Tong, Y.: Divergent evapotranspiration partition
435 dynamics between shrubs and grasses in a shrub-encroached steppe ecosystem, **New Phytologist**,
436 219, 1325-1337, 2018.
- 437 Wei, Z., Yoshimura, K., Okazaki, A., Kim, W., Liu, Z., and Yokoi, M.: Partitioning of evapotranspiration
438 using high-frequency water vapor isotopic measurement over a rice paddy field, **Water Resources
439 Research**, 51, 3716-3729, 2015.
- 440 Wei, Z., Yoshimura, K., Wang, L., Miralles, D. G., Jasechko, S., and Lee, X.: Revisiting the contribution of
441 transpiration to global terrestrial evapotranspiration, **Geophysical Research Letters**, 44, 2792-2801,
442 2017.
- 443 Wen, X., Yang, B., Sun, X., and Lee, X.: Evapotranspiration partitioning through in-situ oxygen isotope
444 measurements in an oasis cropland, **Agricultural and Forest Meteorology**, 230, 89-96, 2016.
- 445 Wu, Y., Du, T., Ding, R., Tong, L., Li, S., and Wang, L.: Multiple methods to partition evapotranspiration
446 in a maize field, **Journal of Hydrometeorology**, 18, 139-149, 2017.
- 447 Xiao, W., Wei, Z., and Wen, X.: Evapotranspiration partitioning at the ecosystem scale using the stable
448 isotope method—A review, **Agricultural and Forest Meteorology**, 263, 346-361, 2018.
- 449 Yakir, D., and Wang, X.-F.: Fluxes of CO₂ and water between terrestrial vegetation and the atmosphere
450 estimated from isotope measurements, **Nature**, 380, 515-517, 1996.
- 451 Yakir, D., and Sternberg, L.: The use of stable isotopes to study ecosystem gas exchange, **Oecologia**, 123,
452 297-311, 2000.
- 453 Yepez, E. A., Williams, D. G., Scott, R. L., and Lin, G.: Partitioning overstory and understory
454 evapotranspiration in a semiarid savanna woodland from the isotopic composition of water vapor,
455 **Agricultural and Forest Meteorology**, 119, 53-68, 2003.
- 456 Yuan, Y., Du, T., Wang, H., and Wang, L.: Novel Keeling-plot-based methods to estimate the isotopic
457 composition of ambient water vapor, **Hydrology and Earth System Sciences**, 24, 4491-4501, 2020.
- 458 Zhang, X. Y., Trame, M., Lesko, L., and Schmidt, S.: Sobol sensitivity analysis: a tool to guide the
459 development and evaluation of systems pharmacology models, **CPT: Pharmacometrics & Systems
460 Pharmacology**, 4, 69-79, 2015.
- 461 Zhang, Y., Shen, Y., Sun, H., and Gates, J. B.: Evapotranspiration and its partitioning in an irrigated winter
462 wheat field: A combined isotopic and micrometeorologic approach, **Journal of Hydrology**, 408,
463 203-211, 2011.
- 464 Zhao, L., Liu, X., Wang, N., Kong, Y., Song, Y., He, Z., Liu, Q., and Wang, L.: Contribution of recycled
465 moisture to local precipitation in the inland Heihe River Basin, **Agricultural and Forest
466 Meteorology**, 271, 316-335, 2019.
- 467 Zhou, S., Yu, B., Huang, Y., and Wang, G.: The effect of vapor pressure deficit on water use efficiency at
468 the subdaily time scale, **Geophysical Research Letters**, 41, 5005-5013, 2014.
- 469 Zhou, S., Yu, B., Zhang, Y., Huang, Y., and Wang, G.: Partitioning evapotranspiration based on the concept
470 of underlying water use efficiency, **Water Resources Research**, 52, 1160-1175, 2016.
- 471
- 472
- 473

474



475 Table 1. Parameters used to estimate the transpiration to evapotranspiration ratio by $F_T(\delta_{ET})$ method and
 476 $F_T(\delta_v)$ method. The underlined data was expurgated because they are outside the possible range of
 477 transpiration to evapotranspiration ratio (i.e., >1).

Date	Time	$\delta_{ET}(\%)$	$\delta_v(\%)$	$\delta_s(\%)$	k(ppm*%)	$\delta_s(\%)$	$C_s(\text{ppm})$	$F_T(\delta_{ET})$	$F_T(\delta_v)$
2017/6/19	7:00	-13.92	-8.06	-28.82	-23593.40	-15.95	14229.25	0.72	0.70
	9:00	-13.70	-7.66	-30.06	-25525.94	-15.26	13062.02	0.73	0.75
	11:00	-13.24	-7.43	-29.22	-33109.69	-15.13	17816.22	0.73	0.73
	13:00	-12.07	-7.57	-29.11	-68684.16	-14.65	20298.32	0.79	0.83
	15:00	-12.03	-7.17	-27.94	-55539.52	-16.30	16264.75	0.77	0.72
	17:00	-12.12	-7.77	-27.75	-74334.03	-17.11	12113.71	0.78	0.84
19:00	-12.87	-8.65	-28.20	-58488.12	-18.68	9569.86	0.78	0.80	
2017/6/25	7:00	-16.14	-8.26	-31.90	43614.44	-15.24	14410.06	0.67	0.58
	9:00	-13.76	-7.66	-30.18	-55954.42	-15.53	15795.70	0.73	0.81
	11:00	-13.11	-7.43	-30.57	-68576.56	-15.31	16896.24	0.75	0.83
	13:00	-13.44	-6.57	-32.25	-50147.02	-15.20	17584.07	0.73	0.78
	15:00	-11.28	-6.17	-31.95	-86993.84	-15.29	19003.64	0.80	0.82
	17:00	-12.20	-7.47	-30.51	-65906.59	-15.58	17323.40	0.79	0.81
19:00	-10.26	-7.85	-29.58	-86035.77	-15.43	12445.80	0.89	0.97	
2017/7/6	7:00	-12.50	-8.66	-34.08	-34129.27	-12.50	13197.35	0.85	0.95
	9:00	-12.49	-8.26	-30.44	-46750.79	-13.67	17075.91	0.81	0.88
	11:00	-11.24	-7.47	-30.02	-71075.34	-13.61	22314.74	0.83	0.87
	13:00	-9.78	-6.08	-28.85	-86554.42	-13.63	25873.61	0.84	0.82
	15:00	-8.14	-5.98	-29.89	-133581.89	-12.54	24659.11	0.91	0.95
	17:00	-9.55	-4.15	-28.85	-24038.31	-12.10	19541.53	0.78	0.73
19:00	-9.85	-6.57	-29.87	-84465.09	-12.95	20679.12	0.86	0.90	
2017/7/15	7:00	-11.26	-7.97	-36.83	-10515.44	-11.60	14008.84	0.89	0.90
	9:00	-10.90	-7.50	-33.55	-16700.50	-12.10	16149.08	0.87	0.86
	11:00	-9.31	-6.47	-29.87	-24921.96	-11.19	18048.50	0.88	0.86
	13:00	-7.46	-5.76	-27.92	-54441.51	-10.20	25313.63	0.92	0.90
	15:00	-8.83	-4.23	-29.03	27456.88	-9.86	26911.28	0.81	0.73
	17:00	-8.89	-4.17	-28.07	64236.29	-8.14	22845.26	0.80	0.72
19:00	-9.04	-7.16	-28.33	-36304.58	-10.00	23204.34	0.91	0.94	
2017/8/2	7:00	-3.82	-9.66	-63.48	-77049.20	-14.99	15582.36	<u>1.11</u>	0.99
	9:00	-12.11	-10.10	-43.83	-45814.72	-14.71	16621.78	0.94	0.94
	11:00	-20.74	-8.61	-37.03	171634.91	-14.46	26197.73	0.57	0.56
	13:00	-11.96	-8.17	-36.00	18843.93	-11.56	25519.20	0.86	0.85
	15:00	-11.55	-7.60	-31.83	-5444.14	-11.65	28032.11	0.84	0.84
	17:00	-10.36	-8.34	-30.89	-63514.27	-12.43	23523.91	0.91	0.94
19:00	-9.70	-8.29	-34.12	-101072.20	-13.58	22204.88	0.95	0.97	
2017/8/13	7:00	-14.56	-9.62	-32.98	7022.82	-15.46	15810.78	0.79	0.73
	9:00	-13.47	-9.34	-34.58	-31496.84	-15.28	18125.23	0.84	0.83
	11:00	-12.69	-8.99	-32.19	-49740.56	-15.15	23377.49	0.84	0.83
	13:00	-9.87	-9.49	-29.73	-149355.24	-16.17	23653.76	0.98	0.98
	15:00	-10.01	-6.87	-28.76	-170549.90	-17.28	25081.47	0.86	0.84
	17:00	-10.82	-8.98	-29.11	-147630.72	-17.46	21800.46	0.91	0.92
19:00	-11.07	-8.42	-29.76	-104132.77	-16.72	17897.72	0.88	0.88	
2018/6/19	7:00	-11.55	-7.66	-42.21	-46373.17	-12.91	12350.75	0.89	0.96
	9:00	-11.57	-7.39	-37.36	-29252.94	-12.62	13438.87	0.86	0.90
	11:00	-15.05	-7.79	-29.30	3109.69	-14.81	13941.85	0.66	0.66
	13:00	-14.12	-8.57	-29.44	-8684.16	-14.72	15936.65	0.73	0.73
	15:00	-10.81	-7.17	-29.72	-36539.52	-13.28	14946.74	0.84	0.84
	17:00	-13.09	-6.47	-28.36	-14334.03	-14.36	14842.84	0.70	0.68
19:00	-9.89	-6.65	-27.47	-48488.12	-15.26	12663.53	0.84	0.77	
2018/7/4	7:00	-12.38	-8.61	-7.55	-8171.10	-12.59	14702.98	<u>1.54</u>	<u>1.22</u>
	9:00	-12.94	-8.45	-26.94	7900.05	-12.69	13414.94	0.78	0.78
	11:00	-12.10	-8.30	-29.18	-14964.90	-12.30	19508.19	0.82	0.85
	13:00	-12.20	-8.89	-20.65	11520.51	-11.96	22917.28	0.72	0.70
	15:00	-11.42	-7.77	-24.37	-5545.77	-12.70	21721.97	0.78	0.72
	17:00	-11.64	-8.48	-20.83	-5165.10	-12.90	18580.88	0.74	0.66
19:00	-11.61	-8.47	-26.37	-16382.76	-12.43	17932.02	0.82	0.83	
2018/7/13	7:00	-7.33	-7.97	-27.66	-67353.64	-11.14	18518.09	<u>1.03</u>	<u>1.02</u>
	9:00	-7.72	-7.50	-22.96	-56621.94	-11.14	19975.82	0.99	0.95
	11:00	-8.82	-7.47	-32.13	-50553.49	-10.50	24384.42	0.95	0.96
	13:00	-10.13	-6.76	-30.15	-30834.35	-10.70	28806.53	0.86	0.88
	15:00	-9.93	-9.23	-32.28	-38742.43	-10.66	29499.65	0.97	0.99
	17:00	-9.84	-8.17	-31.84	-19777.39	-10.20	19535.72	0.93	0.96
19:00	-10.22	-7.16	-28.08	-9873.97	-10.46	15464.54	0.85	0.87	
2018/7/16	7:00	-11.47	-11.66	-23.34	-88769.20	-13.80	16165.60	<u>1.02</u>	<u>1.29</u>
	9:00	-11.17	-11.26	-22.70	-46040.00	-13.93	20925.90	<u>1.01</u>	0.96
	11:00	-12.21	-11.42	-23.03	-32807.57	-13.84	23942.07	0.93	0.91
	13:00	-12.52	-11.09	-23.71	-30703.45	-14.22	29293.09	0.89	0.83
	15:00	-12.21	-9.97	-23.69	3374.13	-12.16	30129.54	0.84	0.83
	17:00	-12.89	-9.11	-20.58	16937.64	-12.34	19370.21	0.67	0.64
19:00	-10.89	-7.51	-22.44	-14501.33	-12.75	13719.02	0.77	0.72	
2018/7/25	7:00	-12.58	-11.26	-20.25	-9352.71	-12.96	21818.45	0.85	0.86
	9:00	-13.69	-12.06	-22.55	-6214.77	-14.03	24953.63	0.84	0.84
	11:00	-12.33	-11.60	-21.72	-34072.08	-13.43	28033.17	0.93	0.94
	13:00	-11.75	-11.10	-19.17	-60112.52	-13.59	33955.04	0.92	0.91
	15:00	-14.90	-11.71	-21.88	18324.12	-12.92	25485.05	0.69	0.81
	17:00	-13.66	-11.27	-30.74	-14127.35	-12.37	22556.53	0.88	0.98
19:00	-15.95	-10.92	-36.17	31405.77	-10.05	19852.51	0.80	0.97	
2018/8/19	7:00	-10.93	-7.49	-39.11	-11535.26	-12.92	16509.69	0.89	0.85
	9:00	-11.99	-8.58	-24.23	869.56	-12.81	14106.31	0.78	0.73
	11:00	-14.72	-10.30	-21.46	15267.54	-14.46	13635.30	0.60	0.53
	13:00	-15.75	-14.69	-16.68	10632.60	-15.18	14099.66	0.47	0.37
	15:00	-14.70	-14.14	-15.44	7750.78	-14.15	14595.20	0.57	0.58
	17:00	-14.51	-11.67	-20.90	70.99	-14.52	12306.90	0.69	0.69
19:00	-13.39	-11.32	-20.52	3667.42	-12.89	11256.45	0.77	0.79	



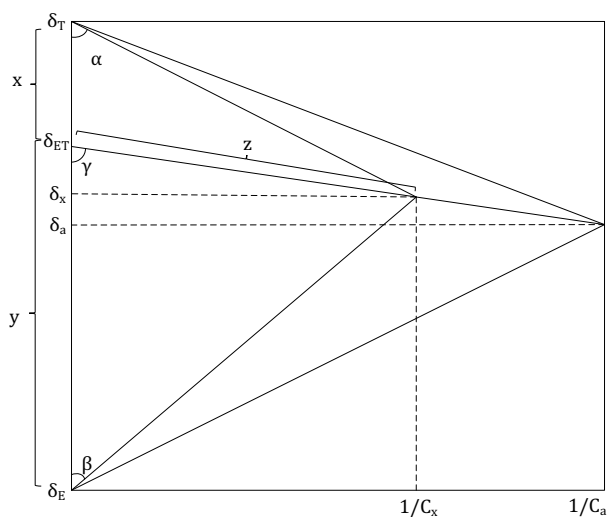
479

480 Fig. 1 Hypothetical graph of the Keeling plot of the isotopic composition of evaporation vapor (δ_E) line
481 (line 1), the isotopic composition of transpiration vapor (δ_T) line (line 2) and the possible area (shaded area)
482 of the Keeling plot lines.

483



484



485

486 Fig. 2 A simplified triangle graph of the Keeling plot. Where x , y and z represent the length of the line

487 segment $(\delta_T - \delta_{ET})$, the line segment $(\delta_{ET} - \delta_E)$ and the line segment $(\delta_{ET} - \delta_x)$, respectively, and α , β and γ

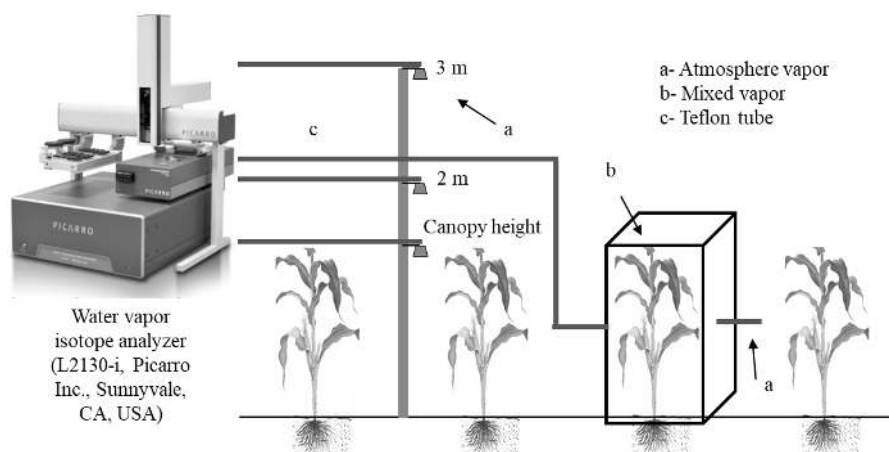
488 represent the angle of the line segment $(\delta_T - \delta_{ET})$ and the line segment $(\delta_T - \delta_x)$, the line segment $(\delta_{ET} - \delta_E)$

489 and the line segment $(\delta_E - \delta_x)$ and the line segment $(\delta_{ET} - \delta_E)$ and the line segment $(\delta_{ET} - \delta_x)$, respectively.

490



491



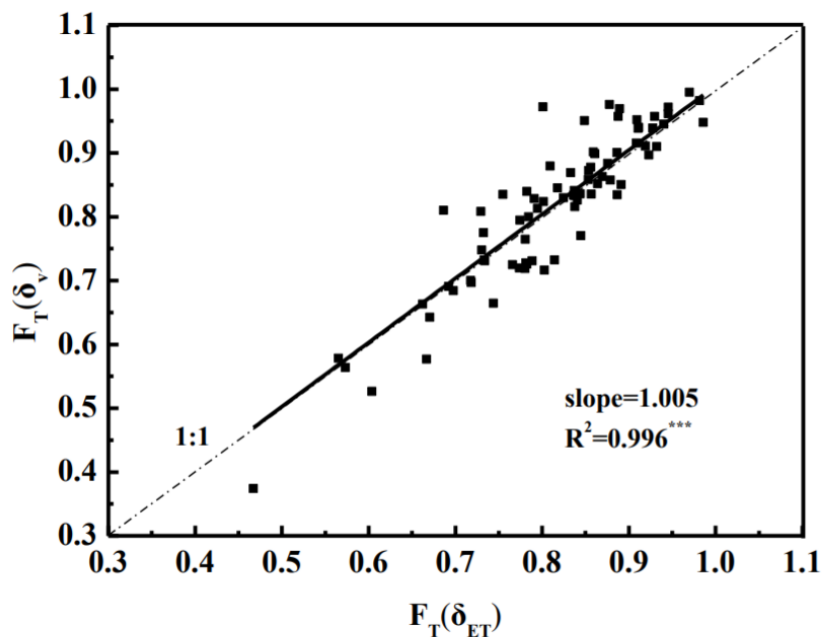
492

493 Fig. 3 Schematic of the plant transpiration chamber system. The system is made up of (a) suction port which
494 absorbs the atmosphere vapor, (b) acrylic glass chamber with volumes of $40 \times 60 \times 180 \text{ cm}^3$, and (c) Teflon
495 tube which connects to the suction port or the chamber with water vapor isotope analyzer.

496



497

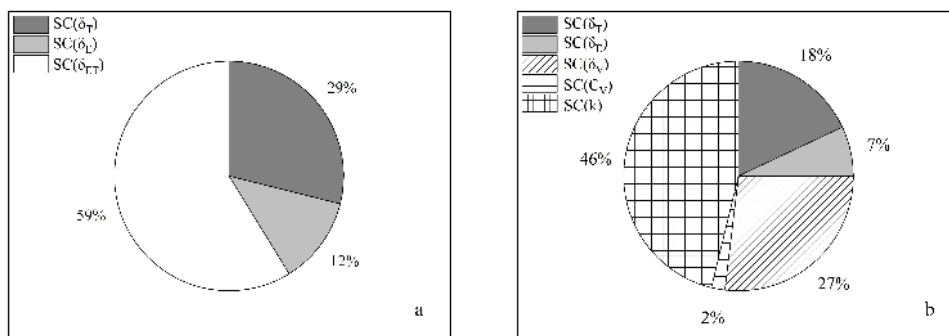


498

499 Fig. 4 Comparison of transpiration fraction in the total evapotranspiration between traditional $F_T(\delta_{ET})$

500 method and the new $F_T(\delta_v)$ method.

501



502

503 Fig. 5 Sensitivity contribution of each parameter based on $F_T(\delta_{ET})$ method (a) and $F_T(\delta_v)$ (b) method,

504 respectively.